Leedale, J, Colley, HE, Gaskell, H, Williams, DP, Bearon, RN, Chadwick, AE, Murdoch, C and Webb, SD

In silico-guided optimisation of oxygen gradients in hepatic spheroids

In silico-guided optimisation of oxygen gradients in hepatic spheroids

Joseph Leedale[1], Helen E. Colley[2], Harriet Gaskell[3], Dominic P. Williams[4], Rachel N. Bearon[1], Amy E. Chadwick[3], Craig Murdoch[2], Steven D. Webb[1,5*]

[1]EPSRC Liverpool Centre for Mathematics in Healthcare, Dept. of Mathematical Sciences, University of Liverpool, Liverpool, L69 7ZL, UK

[2]School of Clinical Dentistry, University of Sheffield, Claremont Crescent, Sheffield, S10 2TA, UK

[3]MRC Centre for Drug Safety Science, Dept. of Molecular and Clinical Pharmacology, University of Liverpool, Liverpool, L69 3GE, UK

[4]AstraZeneca, IMED Biotech Unit, Drug safety & Metabolism, Cambridge Science Park, Cambridge, CB4 0FZ, UK

[5]Dept. of Applied Mathematics, Liverpool John Moores University, Liverpool, L3 3AF, UK

***Correspondence**

Dr Steven D. Webb
Dept. of Applied Mathematics
Liverpool John Moores University
Liverpool L3 3AF
United Kingdom
Tel: +44 (0)151 231 2217
Email: S.D.Webb@ljmu.ac.uk

E-mail addresses:

j.leedale@liverpool.ac.uk (JL); h.colley@sheffield.ac.uk (HEC); hgaskell@uic.edu (HG); dominic.p.williams@astrazeneca.com (DPW); rbearon@liverpool.ac.uk (RNB); aemercer@liverpool.ac.uk (AEC); c.murdoch@sheffield.ac.uk (CM); S.D.Webb@ljmu.ac.uk (SDW).

Abstract

One of the key advantages of assessing the hepatotoxic potential of xenobiotics in spheroids rather than monolayer cell culture is the existence of a more physiologically relevant testing environment. Three-dimensional cultures support spatial gradients in nutrients such as oxygen that can be exploited to better represent *in vivo* gradients that exist along a fundamental sub-unit of liver microarchitecture, the liver sinusoid. The physical and physiological processes that result in the establishment of such gradients can be described mathematically. Quantification of the rates governing these processes and optimisation of cell culture conditions can be performed *in silico* to better inform experimental design. In this study, we take into account cell line-specific physiological properties, spheroid size and the impact of experimental equipment geometries in order to demonstrate how mathematical models can be optimised to achieve specific *in vivo*-like features in different scenarios. Furthermore, the sensitivity of such optimised gradients is analysed with respect to culture conditions and considerations are given to prevent the emergence of hypoxic regions in the spheroid. The methodology presented provides an enhanced understanding of the mechanisms of the system within this simulated *in vitro* framework such that experimental design can be more carefully calibrated when conducting experiments using hepatic spheroids.

Keywords: Liver spheroids; HepG2; HepaRG; Hypoxia; Oxygen gradient; In silico modelling.

1 Introduction

Two-dimensional (2D) cell culture systems have been extensively used to enhance our understanding of human biology with applications ranging from the study of pathophysiology at the cellular level to the pharmacology and toxicology of novel drugs. However, there remains a considerable disparity between *in vitro* experimental findings and *in vivo* relevance, motivating the need for improved *in vitro* methods. The enhanced physiological relevance of three-dimensional (3D) *in vitro* models provides an important link between 2D *in vitro* models and *in vivo* whole-body biology (Yamada & Cukierman, 2007). While many 3D model systems, from scaffold-based models to microfluidic bioreactors, are now being employed to increase translational applicability, the use of spheroid models in particular has become progressively important to fundamental medical research and safety assessment (Kyffin et al., 2018). 3D spheroids represent a convenient and versatile *in vitro* model that improves physiological relevance, cell morphology and functionality (compared to 2D systems), yet are simple to deploy, cost-effective and amenable to higher throughput techniques. Although these systems inevitably lack certain physiological complexities (e.g. vasculature) as a consequence of their relative simplicity, other features such as *in vivo*-like gradients can be established with the move to three dimensions. Of paramount importance in these physiological gradients is oxygen.

Physiological oxygen gradients are a prime example of homeostasis within healthy cells and tissues and significant disruption to oxygen availability can lead to apoptosis and necrosis. Hypoxia is a prevalent feature in the growth stages of solid tumours due to the rapid growth characteristic of mutated cancer cells causing an abnormal distribution of cells and nutrient-supplying blood vessels (Vaupel et al., 1989, Muz et al., 2015). As cancer cells typically proliferate more rapidly than normal cells, a tumour mass is soon formed that is unable to be adequately supplied by the surrounding vasculature, that also tends to be immature and poorly

formed. A hypoxic region is formed in the centre of the tumour due to the distance between the oxygen supply and this core of cells. This process is symptomatic of an early-stage tumour, otherwise known as an avascular tumour, as the tumour has not yet induced the production of its own blood vessel network (Brown & Giaccia, 1998, Riffle & Hegde, 2017). Similarly, hyperoxic conditions can lead to the generation of reactive oxygen species and oxidative stress, and thus there exists a bounded range of oxygen tensions that is functionally optimal for each tissue (Carreau et al., 2011, Lee et al., 2014). Avascular tumours are studied experimentally by culturing cancer cells as spheroids as they share similar growth kinetics (Freyer, 1988, Grimes et al., 2016). The avascular phase of the life cycle of a tumour covers the initial mutations of normal cells through to a diffusion-limited steady state where the tumour's growth is limited by a balance between nutrient consumption and nutrient supply via diffusion. Mathematical modelling can facilitate the refinement and optimisation of *in vitro* studies to more accurately translate these results to a more physiologically realistic *in vivo* scenario (Williams et al., 2013). The importance of understanding the local environment and mechanisms within tumour spheroids to develop medical applications has led to considerable mathematical modelling efforts in this area. Some work has focused on reproducing growth and development processes (Chaplain, 1996, Grimes et al., 2016), while others investigate the effects of various oxygen consumption kinetics in different geometries and hypoxic environments (Grimes et al., 2014b, Grimes et al., 2014a, Leedale et al., 2014). Acknowledgement of the importance of spatial dynamics in spheroids has also led to mathematical models that simulate 3D pharmacological processes such as drug delivery and metabolism (Ward & King, 2003, Mehta et al., 2012).

The spatial heterogeneity, or zonation, observed in tumours is a key characteristic that must be addressed when modelling these systems. These spatial features are also an essential characteristic of other physiological environments such as the primary detoxification system of the body, the liver, and in particular the hepatic lobule and liver sinusoid (Jungermann &

Kietzmann, 2000). The spatial gradients that exist within the sinusoid microenvironment impact upon overall hepatocyte function, metabolic capabilities and susceptibility to toxins with respect to location (Lee-Montiel et al., 2017). Therefore, cellular spheroids provide effective *in vitro* tools to study the pharmacological and toxicological effects of drugs in the liver throughout the local microenvironment by replicating physiologically relevant features within these 3D structures.

The oxygen gradient is a key characteristic of the liver sinusoid that must be maintained in spheroids in order to preserve this *in vivo*-like zonation (Figure 1), which ranges from 65 mmHg in the periportal region of the sinusoid to 35 mmHg at the central vein (Jungermann & Keitzmann, 1996, Jungermann & Kietzmann, 2000). The oxygen gradient is primarily dependent on the supply of oxygen, flow rate, length of sinusoid and cellular uptake. For *in vitro* spheroid models that do not include flow, their size can theoretically be optimised in order to recapitulate the same range of oxygen concentrations from boundary to core. This range would then provide the appropriate environment to make the test system more comparable when studying effects of cell function and spatial variation in metabolism between periportal and perivenous (centrilobular) regions. Indeed, the role of the oxygen gradient in regulating metabolic zonation is critically important for pharmacological studies, whether or not this regulation is direct or via downstream signalling (Kietzmann, 2017). The supply of oxygen *in vitro* is dependent on the externally controlled atmosphere, type and volume of culture media (which can be controlled *in vitro*), and diffusion of oxygen through the media and spheroid. The length of sinusoid, which is assumed to be constant and regular *in vivo*, is effectively represented by the radius of the *in vitro* spheroid. All of these parameters that determine the hepatic oxygen gradient *in vitro* can be optimised using a suitable mathematical model.

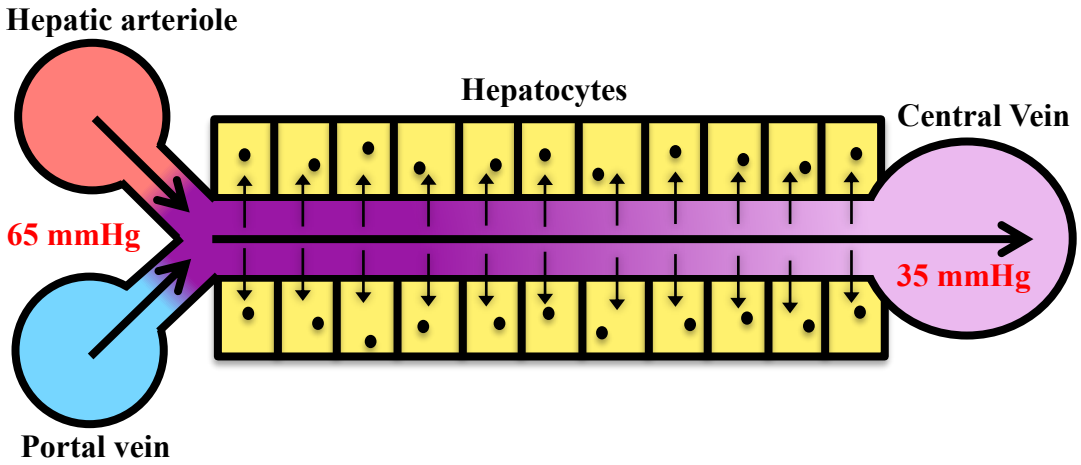

Figure 1: **A schematic representation of the liver sinusoid.** Mixed blood from the portal vein and the oxygen-carrying hepatic arteriole flows towards the central vein where it is drained from the liver lobule. As blood flows from the periportal region to the perivenous (centrilobular) region, oxygen is removed from the blood by hepatocytes establishing an oxygen gradient ranging from 65 mmHg (periportal) to 35 mmHg (perivenous).

2 Materials and methods

2.1 Model derivation

2.1.1 Model I: Spheroid only

The mathematical model of spatiotemporal oxygen dynamics throughout the spheroid includes diffusion and oxygen uptake terms in a continuum approach. We assume that oxygen consumption is dependent on the local oxygen concentration in a non-linear manner such that the consumption rate saturates for higher oxygen levels. Therefore, we describe the oxygen dynamics within the spheroid using the following partial differential equation (PDE):

$$\frac{\partial C}{\partial t} = D_1 \nabla^2 C - \frac{V_{max} C}{C + K_m}, \qquad \boldsymbol{x} \in \Omega. \tag{1}$$

Oxygen concentration (mol/m^3) is represented by C, D_1 is the diffusion rate constant in m^2/s (assumed to be independent of radial position), V_{max} is the maximum consumption rate in

mol/m^3/s and K_m represents the oxygen concentration at which consumption is half maximal (mol/m^3). Time is given by t while $\boldsymbol{x}$ represents the spatial vector with the equation being considered within domain Ω (the spheroid). Since we will be looking at oxygen dynamics that occur on a much faster timescale than cell cycle dynamics (growth and division) we assume the radius of the spheroid to be constant, R. The system is assumed to be at steady state in a radially symmetric sphere (see Figure 2A) and is presented in spherical coordinates in equation (2) so that the problem is reduced to a 1-dimensional equation in variable r, the radial coordinate. The following system (writing the Laplacian operator with respect to the radial coordinate) is used to describe steady state spatial oxygen dynamics in a radially-symmetric sphere:

$$\frac{D_1}{r^2}\frac{\partial}{\partial r}\left(r^2\frac{\partial C}{\partial r}\right) - \frac{V_{max}C}{C+K_m} = 0, \qquad r \leq R, \tag{2}$$

$$\frac{\partial C}{\partial r} = 0, \qquad r = 0. \tag{3}$$

The concentration of oxygen at the boundary of the sphere is fixed such that

$$C = C_R, \qquad r = R. \tag{4}$$

Initially the oxygen concentration is given by $C(r,0) = C_R \; \forall \, r \in \Omega$.

2.1.2 Model II: Spheroid in well

Model I requires the oxygen concentration at the spheroid boundary to be fixed at a physiologically relevant value (periportal blood/65 mmHg). However, this is difficult to calibrate *in vitro* since oxygen is not directly controlled at this region. The oxygen concentration at the boundary of a spheroid cultured *in vitro* is dependent on multiple local environmental factors such as external oxygen concentration at the air/media interface, diffusion rate of oxygen within the media, and the volume of media used. Furthermore, the

mathematical problem is not simply radially symmetric in 3D spherical coordinates due to the geometry of the equipment used for cell culture, i.e. the physical structure of the well, and the position of the spheroid. To represent these features, we have developed Model II based on the *in vitro* geometry of Ultra-Low Attachment (ULA) plate wells with media (see Figure 2B). Similar geometrical features are also relevant for other standard culture systems such as agarose-coated 96 well plates, although these may exhibit more variation due to the formation of the agarose layer. Therefore, we impose ULA plate geometry for more consistency within the mathematical model simulations. Understanding the impact of culture conditions and geometry on oxygen dynamics is known to be critical in order to maintain hepatocyte viability and functionality *in vitro* and has previously been modelled for 2D monolayers (Yarmush et al., 1992). Model II is therefore an extension of Model I used to take into account a representative 3D *in vitro* environment and associated geometries.

Model II incorporates a realistic *in vitro* environment within the model geometry such that oxygen dynamics are modelled in cylindrical coordinates with radial symmetry about the axis through the centre of the well. Therefore, the steady state spatial oxygen dynamics within the hepatic spheroid are governed by the following PDE:

$$\frac{D_1}{r}\frac{\partial}{\partial r}\left(r\frac{\partial C}{\partial r}\right) + D_1\frac{\partial^2 C}{\partial z^2} - \frac{V_{max}C}{C + K_m} = 0. \quad (5)$$

Note that this mathematical representation could be more broadly applied to oxygen dynamics in other cell-based spheroids with appropriate changes in model parameterisation. In Model II, oxygen concentration in the media outside the spheroid is also considered, where there is no consumption and simple diffusion governs the spatial dynamics. Oxygen diffuses at a rate, D_2, in the outer medium and thus we have the following equation to represent oxygen dynamics outside the sphere:

$$\frac{D_2}{r}\frac{\partial}{\partial r}\left(r\frac{\partial C}{\partial r}\right)+D_2\frac{\partial^2 C}{\partial z^2}=0, \tag{6}$$

Oxygen concentration is fixed at the air/media interface boundary condition, $C = C_A$, while zero-flux boundary conditions are imposed at all other boundaries of the geometry (walls of the well), i.e., $\nabla C \cdot \mathbf{n} = 0$, where $\mathbf{n}$ is the outward-pointing unit normal vector. Initial conditions are given by $C(r, z, 0) = C_A$. In between the two phases at the boundary of the sphere, $r = R$, we assume continuity in C such that

$$C_{int} = C_{ext}, \qquad r = R. \tag{7}$$

where C_{int} here represents the concentration of oxygen at the interior of the spheroid/media interface and C_{ext} represents oxygen at the exterior. It is also assumed that the flux is equal such that mass is conserved, i.e.,

$$D_1\frac{\partial C_{int}}{\partial r} = D_2\frac{\partial C_{ext}}{\partial r}. \qquad r = R. \tag{8}$$

A **B**

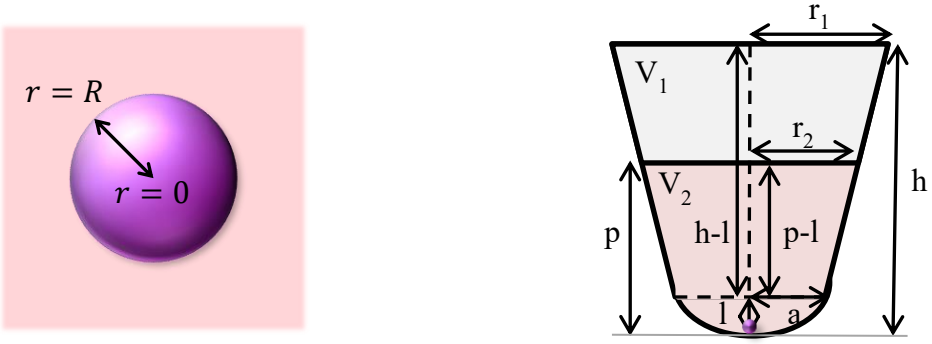

Figure 2: **Model geometry schematics.** Hepatic spheroids are formed *in vitro* via media incubation whereby the hepatocytes initially seeded aggregate to form uniform spheroids. (A): Representative Model I schematic of an idealised radially symmetric spheroid. (B): Representative Model II schematic of a typical Ultra-Low Attachment (ULA) plate well with media. The oxygen concentration experienced by the cells is dependent on external concentration in the air and depth of the media. Spheroid position and environmental geometry are indicated corresponding to measurements provided in Table 1.

Symbol	Description	Value
V_1	Well volume	360 µl
V_2	Media volume	100 µl
r_1	Well radius (top)	3.429 mm
h	Depth of well	11.303 mm
a	Well radius (bottom)	3.175 mm
l	Height of spherical cap	1.6 mm
r_2	Media radius (top)	3.2338 mm
p	Media depth	3.848 mm

Table 1: Physical measurements of the geometry of a typical Ultra-Low Attachment (ULA) plate (Costar® 96-well Ultra Low Attachement (Corning Life Sciences, 2018)) with media, used to culture hepatic spheroids *in vitro* (see corresponding schematic in Figure 2B).

2.2 Model parameterisation

Oxygen consumption parameters (V_{max} and K_m) for human hepatocellular cell lines were obtained using Seahorse Technology, which monitors oxygen consumption rates (OCR) and extracellular acidification rates (ECAR) in live cells to determine bioenergetic behaviour. The Seahorse experiments carried out by Kamalian et al. (2018) yielded a panel of OCR values for both HepaRG and HepG2 cell types. The maximum oxygen consumption rates (corresponding to V_{max} in the *in silico* modelling) were derived by summing the mean non-mitochondrial and maximal respiration OCR values. These rates were presented per 10,000 cells and thus an average hepatocyte volume of 3.4×10^{-15} m^3 (Lodish et al., 2000) was used to convert OCR to the desired units for V_{max} ($mol/m^3/s$). Maximum consumption rates were therefore calculated as V_{max} = 4.40×10^{-2} $mol/m^3/s$ for HepaRG cells and V_{max} = 1.54×10^{-2} $mol/m^3/s$ for HepG2 cells. It is possible that OCR measured in different cell culture conditions (2D, 3D, suspension, etc.) may cause the exact value to vary. However, it should be noted that the values used in the model appear feasible for the system and are the same order of magnitude as V_{max} values found

in other multicellular spheroid studies (Leedale et al., 2014, Lesher-Pérez et al., 2017). The Michaelis constant appears to be more difficult to ascertain as only measurements based upon rat studies have been made. For this study we use the value for primary rat hepatocytes, K_m = 6.24×10^{-3} mol/m^3 (Shipley et al., 2011), itself comparable to values used in other studies and models, based upon rat hepatocytes cultured using a variety of methods (Buerk & Saidel, 1978, Yarmush et al., 1992, Foy et al., 1994, Colton, 1995, Allen & Bhatia, 2003, Mattei et al., 2017).

To determine oxygen transport parameters, the rate of oxygen diffusion through the spheroid was derived based on the modelling results of Leedale et al. (2014). This previous model assumed linear oxygen consumption kinetics and optimised parameter values by fitting to oxygen distributions in cellular spheroids, measured under various external oxygen conditions. We repeated the optimisation procedure, using the same data, but for the radially symmetric diffusion model with saturating uptake (identical to equations (2)), acquiring a better fit and updated diffusion coefficients. The diffusion rate of oxygen inside the sphere, D_1, was estimated to be 1.60×10^{-9} m^2/s and the rate outside the sphere, D_2, is 4.85×10^{-9} m^2/s.

In Model I we prescribe our fixed boundary concentration to be equivalent to the concentration of oxygen at the periportal region of the sinusoid, C_R = 65 mmHg (~8.6% O_2). In Model II we prescribe the external far-field concentration to be equivalent to atmospheric oxygen concentration, i.e., C_A = 160 mmHg (~ 21% O_2).

2.3 Numerical simulation

Model II PDE solutions were obtained using COMSOL Multiphysics® software. All other simulations and plotted model outputs were obtained using MATLAB.

2.4 Cell culture and generation and immunohistochemical staining for hypoxia

The asymmetry of oxygen distribution during spheroid culture *in vitro* was motivated and supported by an illustrative example of immunohistochemical staining and so we provide the experimental details here for completeness. The human hypopharyngeal carcinoma cell line, FaDu (American Type Culture Collection) (Rangan, 1972) were cultured in RPMI-1640 medium supplemented with 10% (v/v) fetal calf serum (BioSera), 2 mM L-Glutamine, 100 IU/ml penicillin and 100 µg/ml streptomycin (Sigma) at 37°C in 5% CO_2. Tumour spheroids were generated from FaDu cells using the liquid over-lay method as previously described (Colley et al., 2014). Briefly, 100 µl of 1.2 x 10^5/ml FaDu cells were added to each well of a 96-well plate coated with 1.5% type V agarose (w/v in DMEM) and incubated at 37°C, 5% CO_2. Medium was changed every 48 h by removing and re-placing 50% of the medium. Images of MCTS were captured using a Zeiss Axiovert 200M inverted microscope fitted with a Nikon AxioCam digital camera and spheroid diameter measured using Axiovision 4.6 software. For visualisation of hypoxic regions, spheroids were incubated with 170 µM Hypoxyprobe (Hypoxyprobe, MA) for 2 hours, washed with PBS, fixed in 4% paraformaldehyde, embedded in agarose (1.5% w/v in 10% PBS-buffered formalin), histologically processed and embedded in paraffin wax. Sections (5 µM) of wax-embedded spheroids were dewaxed, rehydrated and endogenous peroxidase neutralised with 3% hydrogen peroxide in methanol for 20 minutes. Following antigen retrieval with 1% pronase, tissue sections were blocked for 20 minutes at room temperature with 3% bovine serum albumin and incubated with mouse anti-hypoxyprobe monoclonal antibody for 1 h at room temperature. Secondary antibody and avidin-biotin complex provided with Vectastain Elite ABC kit (Vector Laboratories) were used in accordance with the manufacturer's instructions. Finally, NovaRed (Vector Laboratories) was used to visualise hypoxia. Sections were counterstained with 4',6-Diamidine-2'-phenylindole dihydrochloride (DAPI; Sigma) and mounted with Prolong™ Gold Antifade (Life

Technologies). Fluorescent images were captured using a spinning disc confocal microscope (Olympus IX81).

3 Results

3.1 Model I: Recapitulation of the in vivo sinusoid gradient by fixing the oxygen concentration at the sphere boundary

The steady state solution for Model I with a HepaRG spheroid radius of 150 μm and fixed periportal (boundary) supply of 65 mmHg is plotted in Figure 3 such that the simulated distribution of oxygen concentration across the radial distance of the spheroid at equilibrium can be visualised. Physiologically relevant oxygen concentrations of oxygen within a sinusoid microenvironment are indicated including desired *in vivo* oxygen values at the sinusoid extrema and a value corresponding to hypoxia, defined as 10 mmHg (Martinez et al., 2008). Under these conditions, the *in vivo* sinusoid gradient is not replicated with the *in silico* model since there is too little oxygen present in the central region of the spheroid. This would suggest that the size of the spheroid is suboptimal in this scenario and therefore the spheroid radius (R) was optimised in order to ensure the relevant oxygen concentration at the spheroid core, i.e., $C(0)$ = 35 mmHg.

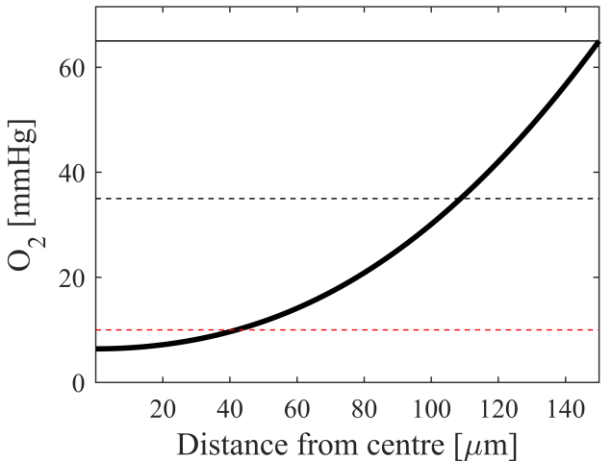

Figure 3: **Simulation of Model I showing the spatial distribution of oxygen concentration at steady state in an *in silico* hepatocyte spheroid of radius 150 μm with radial symmetry.** Physiologically significant concentrations of oxygen concentration are indicated with horizontal lines representing the periportal region (black, solid), perivenous region (black, dashed) and threshold for hypoxia (red, dashed).

Figure 4 shows how varying the radius of both HepaRG and HepG2 spheroids can be effectively implemented within the model in order to ensure that the desired oxygen gradient across the spheroid (*in silico* sinusoid) is obtained and similarly, in order to predict at what radius the spheroids are likely to experience hypoxia in the spheroid core (*in silico* central vein). HepaRG spheroids have *in vivo*-like oxygen values at the centre when they are approximately 100 μm in radius. The corresponding optimal radius for HepG2 spheroids is approximately 170 μm. Hypoxia is predicted in the spheroid interior when the radii is greater than 142 μm in HepaRG spheroids and 241 μm in HepG2 spheroids.

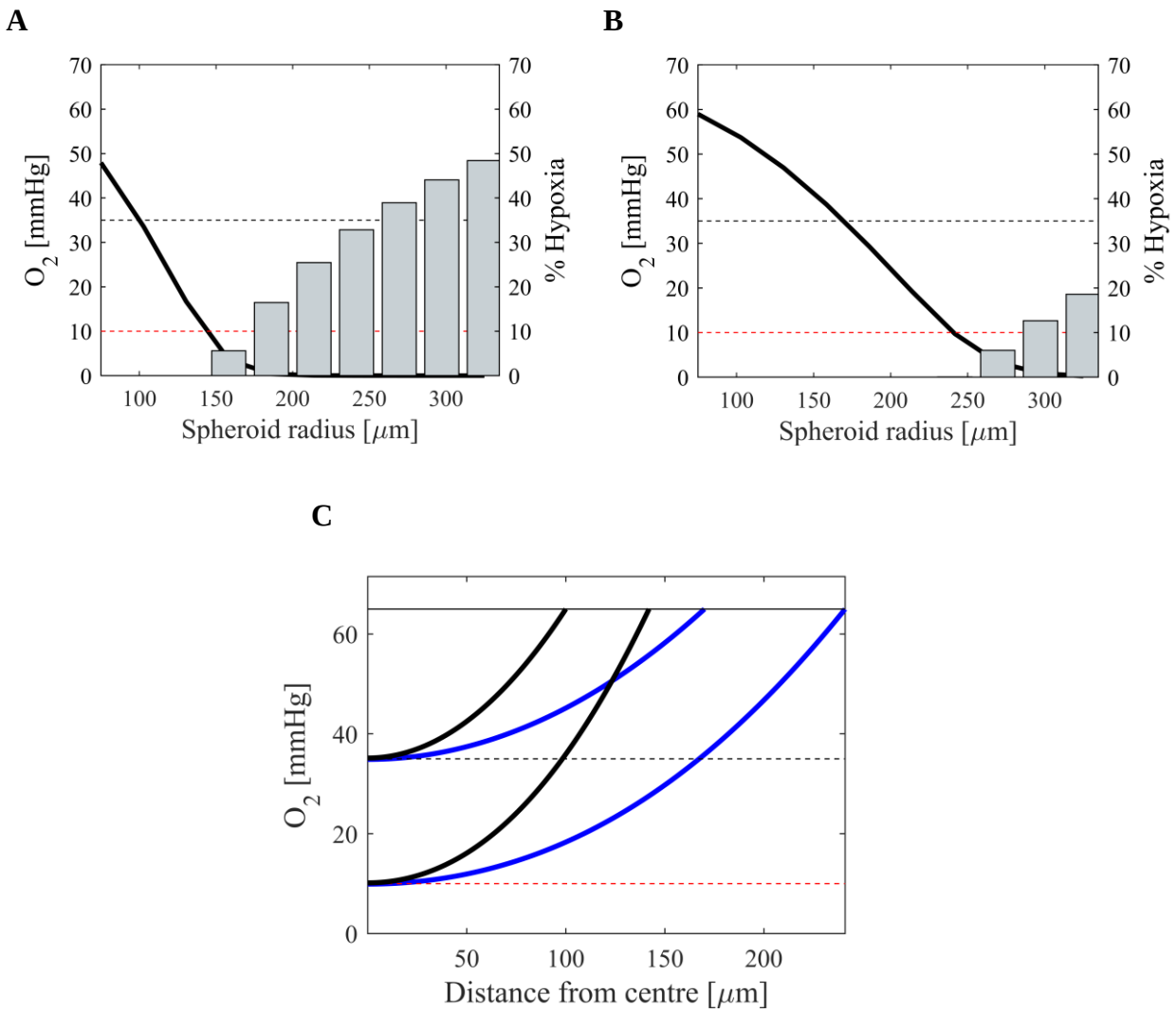

Figure 4: **Mathematical model predictions of optimal sinusoidal oxygen gradients and hypoxia for hepatocyte spheroids.** Oxygen concentration at the spheroid centre (i.e., "central vein") is plotted for a range of spheroid radii (black, bold) for both HepaRG (A) and HepG2 (B) cells. Physiologically relevant oxygen concentrations are denoted with horizontal lines for *in vivo* central vein oxygen concentration (black, dashed) and hypoxia (red, dashed). Grey bars represent the percentage of hepatocytes in the spheroid that are hypoxic as radii are increased. (C): Oxygen concentration profiles for optimal spheroid radii and hypoxic spheroid radii are plotted against the radial distance from the spheroid centre for both HepaRG (black) and HepG2 (blue), with physiologically relevant concentrations denoted.

Whereas HepaRG simulations appear realistic in terms of the often cited ~150 μm oxygen diffusion distance, the estimated size at which HepG2 spheroids begin to suffer central hypoxia appears to be quite large (Carmeliet & Jain, 2000, Glicklis et al., 2004, Anada et al., 2012). However, it should be noted that there is evidence that different cell types have different metabolic demands (Olive et al., 1992) and therefore, all else being equal, it is expected that

optimal spheroid size should in fact vary with a variation in oxygen consumption kinetics, as governed by the physical processes described in our mechanistic model. We are not aware of any exact measurements of local pO_2 in HepG2 spheroids but it has been shown that HepG2 cells consume oxygen at a much lower rate than primary hepatocytes (Nyberg et al., 1994). Furthermore, our definition of hypoxia ($C < 10$ mmHg) may be overly prescriptive compared to other studies, e.g. 40 mmHg (Curcio et al., 2007), and we do not account for other environmental factors (i.e., pH, glucose, etc.) or cell death as indicators for limitations in spheroid size - only the physical processes of oxygen diffusion and consumption. In light of these considerations we opt to carry out the rest of our investigation based on the HepaRG cell line to focus on the impact of well geometry on oxygen dynamics in the *in vitro* spheroid system, but stress that attention should be paid to different cell line metabolic demands when considering optimal size for recapitulation of hepatic O_2. Moreover, the HepaRG cell line is potentially more relevant for optimisation since these spheroids do not proliferate once differentiated and more closely resemble *in vivo* functionality (Gunness et al., 2013).

3.2 Model II: Recapitulation of the in vivo sinusoid gradient within a representative in vitro environment

Model II adopts radial symmetry in cylindrical coordinates, with the central vertical axis of the well (top-to-bottom) representing the central axis of symmetry, and takes into account the diffusion of oxygen through the media as well as inside the hepatocytes as before. The output of Model II differs to Model I in two key ways. Firstly, the oxygen concentration at the boundary of the spheroid is no longer explicitly specified and imposed as a constant value, but rather depends on the concentration at the media-air interface (atmosphere) and subsequent dynamic effects of diffusion through the media, flux into the spheroid and consumption within the spheroid. Secondly, the spatial oxygen dynamics within the spheroid are no longer symmetrical about the centre of the spheroid due to the position of the spheroid within the well

and the location of the oxygen source, at the top of the well (Figure 5). This asymmetric distribution of oxygen concentration is supported experimentally by observed distributions of hypoxia within spheroids in culture (e.g., see hypoxic FaDu spheroid in Figure 6C). By quantifying regions of hypoxia using relative light units, it is clear that more hypoxic conditions are observed towards the bottom of the *in vitro* spheroid (Figure 6D-E). The asymmetry within the hepatic spheroid of the *in silico* model can be visualised more clearly by a 1D representation of the spatial oxygen dynamics through a central axis of symmetry cross-section (Figure 6A-B). It is clear from this representation that the minimum oxygen concentration is not found at the centre of the spheroid but at a distance closer to the bottom of the well. For example, under the modelling conditions of a HepaRG spheroid of radius 150 μm in 100 μl of media, the minimum oxygen concentration is predicted to be approximately 16 mmHg at 129 μm from

the bottom of the well (i.e., ~20 μm away from the core, at the distal side of the spheroid, relative to the oxygen source).

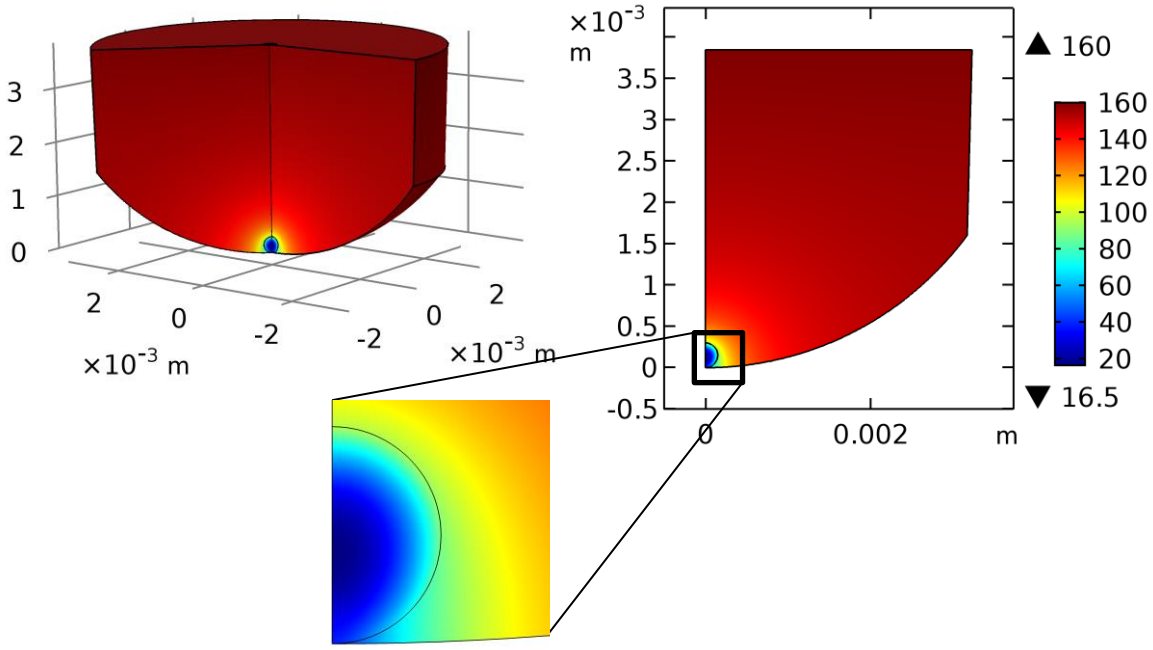

Figure 5: **Simulated 3D spatial oxygen dynamics within the *in vitro* culture environment**. Model II simulation results for a geometrically relevant environment to represent the spatial distribution of oxygen concentration for hepatic spheroids cultured *in vitro*. The model output represents the steady state solution for a HepaRG spheroid of radius 150 μm in 100 μl of media. The results can be visualised in 2D due to the axisymmetric nature of the problem and the region containing the hepatic spheroid is highlighted for clarity.

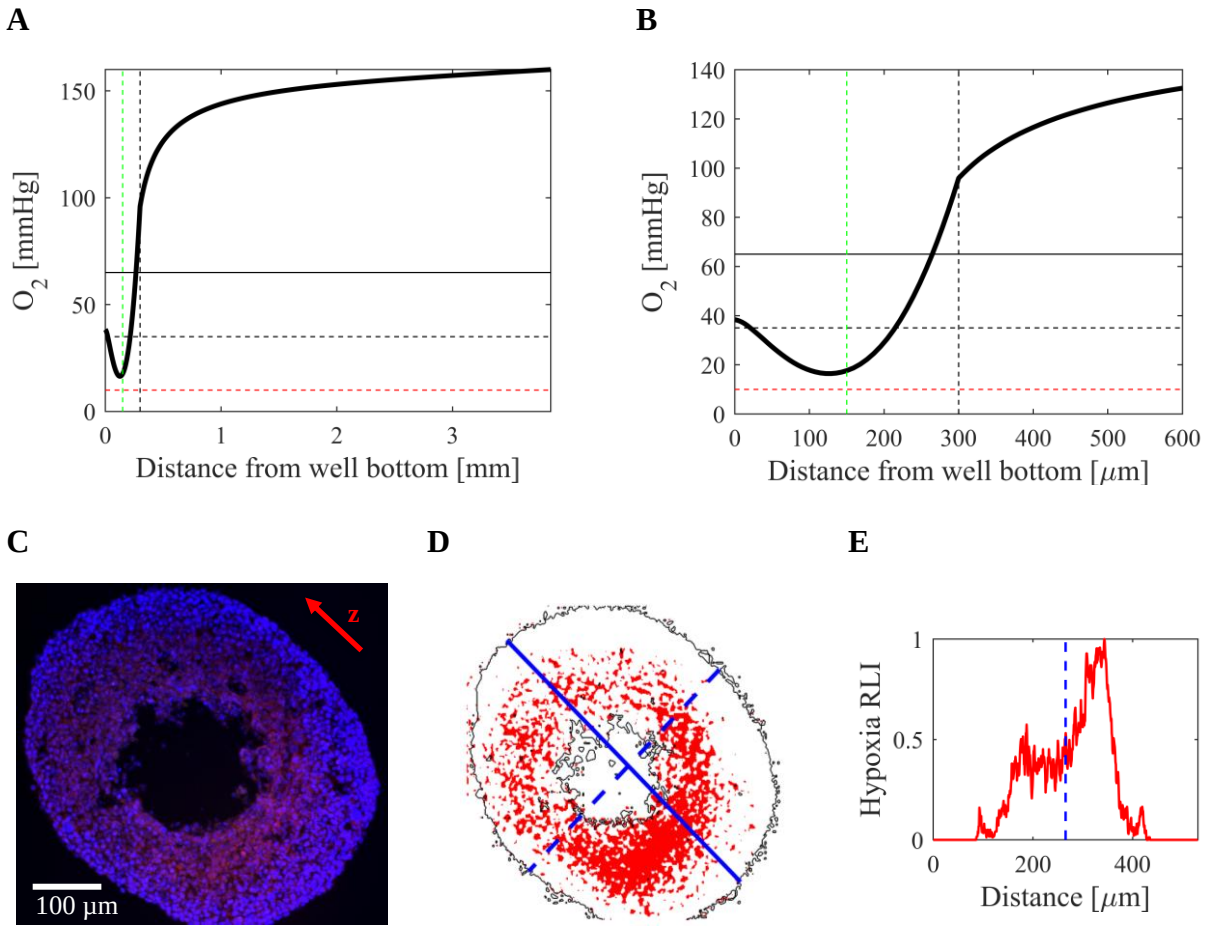

Figure 6: **1D cross-section of spatial oxygen dynamics.** (A): 1D cross-section of the model simulation described in Figure 5 with respect to the axisymmetric z-axis (represented as distance from the bottom of the well). (B): The same results are plotted for a reduced spatial range to visualise oxygen dynamics within the spheroid more clearly. Solid and dashed horizontal black lines indicate desired oxygen concentrations for periportal and perivenous zones within the liver. Horizontal red dashed lines represent the threshold for hypoxia. Vertical green dashed lines represent the centre of the spheroid. Vertical black dashed lines represent the spheroid boundary. (C): Example of an *in vitro* spheroid exhibiting asymmetrical oxygen distribution. Image represents immunohistochemical staining of a hypoxic FaDu spheroid with cell nuclei indicated in blue and hypoxia in red. The red arrow indicates a representative z-axis. (D): Spatial plot of the relative light intensity (RLI) of hypoxia within the spheroid. Blue lines indicate the representative z-axis relative to the bottom of the well (solid) and a cross-section through the centre of the spheroid (dashed, for comparison with (E)). (E): Hypoxia RLI versus distance from the top of the spheroid. RLI (red) is calculated for each position along the z- axis from the top to the bottom of the spheroid. The spheroid centre is also indicated (blue dashed line).

Ideally, in order to optimise the *in vitro* system to be more representative of the hepatic oxygen range observed *in vivo*, the maximum oxygen concentration within the spheroid would

correspond to that in the periportal blood and the minimum oxygen concentration would correspond to that in the perivenous blood. One experimentally convenient method to vary the local oxygen concentration experienced by the spheroid is to adjust the media volume. Thus, the identification of optimal conditions for replicating the desired oxygen gradient can be investigated by comparing variations in both media volume and spheroid radius. By calculating the steady state solutions of Model II for a relevant range of media volumes (50-300 μl) and spheroid radii (100-250 μm), the oxygen concentrations at specific locations within the geometry can be compared for optimisation (Figure 7). The two primary quantities of interest are the maximum oxygen value at the spheroid boundary (Figure 7A) and the minimum concentration within the spheroid (Figure 7C). We also calculate an average oxygen value (Figure 7B) in acknowledgement of the heterogeneity across the boundary (e.g., see Figure 5). Spheroid-radius/media-volume parameter combinations are optimised by identifying the values that provide the desired oxygen concentration in each region, indicated by solid white contours in Figure 7. A dashed white contour in Figure 7B also denotes at which radii/volume hypoxia is predicted to occur within the spheroid. The variation in oxygen concentrations appears to be more significant with spheroid radius rather than media volume, and so this parameter is deemed more sensitive within these relevant physical ranges.

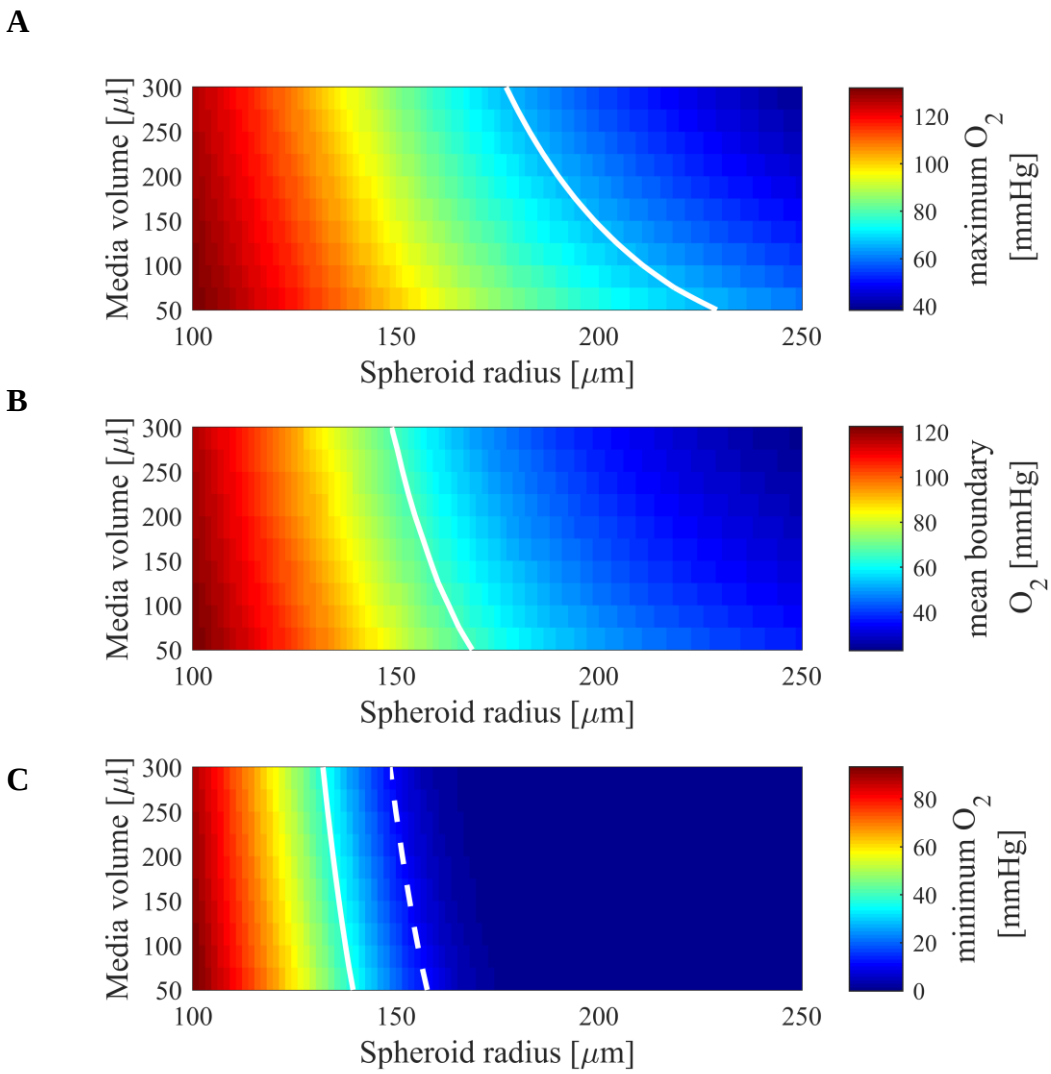

Figure 7: **Identification of *in vivo* oxygen concentrations for different *in vitro* culture conditions in two distinct spheroid regions.** Steady state oxygen concentrations are calculated for a range of spheroid radii and media volumes representing the maximum (A) and average (B) spheroid boundary values, and the minimum values within the spheroid (C). Solid white contours represent the curve along which the oxygen concentration is equal to the desired *in vivo* value for periportal (A, B) and perivenous (C) regions. The dashed white contour indicates which spheroid radius and media volume combinations lead to hypoxia within the spheroid as predicted by the mathematical model.

For a given spheroid radius, the mathematical model can suggest what amount of media volume leads to physiologically relevant oxygen concentrations at the boundary and at the minimum. However, it should be noted that the two optimal contours provided in Figure 7 do not intersect within the relevant ranges of radius and volume parameters. This is more clearly indicated in

Figure 8, where the contours are collated onto the same plot. Therefore, in order to optimise the *in vitro* system within these physical ranges, it is not possible to simultaneously satisfy both conditions for the desired *in vivo* gradient, and thus an intermediate region in parameter space must be identified which optimally satisfies the problem with minimum error. The percentage error associated with each combination of spheroid radius and media volume is calculated by combining the absolute differences at both the maximal spheroid boundary and minimum oxygen value within the spheroid according to the following formula:

$$\text{Combined \% error} = \frac{1}{2}\left(\frac{|C_{max} - C_{PV}|}{C_{PV}} + \frac{|C_{min} - C_{CV}|}{C_{CV}}\right) \times 100 \quad (9)$$

This error is plotted across the parameter space in Figure 8A and the minimum error can subsequently be identified, corresponding to a spheroid of radius 131.82 μm and media volume of 300 μl. The 1D oxygen profile for this parameterisation can be seen in Figure 8B. Note that even a significant increase in media volume yields little improvement in the minimisation of the combined % error (e.g., a media volume of 600 μl, with spheroid radius of 127.27 μm, decreases the error from 27.2% to 23.6%, and the contours do not intersect for media volumes up to 5×10^4 μl – data not shown). In Figure 8B, the compromised oxygen gradient can be clearly visualised whereby the minimal oxygen concentration is optimal and well above the hypoxic threshold, but the maximal, and even the average oxygen concentration around the spheroid boundary (indicated in red), are above the desired periportal value. Nevertheless, these optimal values provide a range of oxygen values which encompass the desired sinusoid gradient. However, analysis of the sensitivity of the model discrepancy to perturbations in these optimal parameters reveals that the HepaRG spheroid is a sensitive system, with a 20% decrease in the spheroid radius (~105 μm) leading to a +69% average error in the optimal oxygen values and a 20% increase in the spheroid radius (~158 μm) resulting in a -57% average

error (Figure 9). Furthermore, it should be noted that, in this scenario, the model predicts that an increase in radius of just 17.18 μm (or measurement error of 17.18 μm) will lead to the onset of hypoxia within the spheroid.

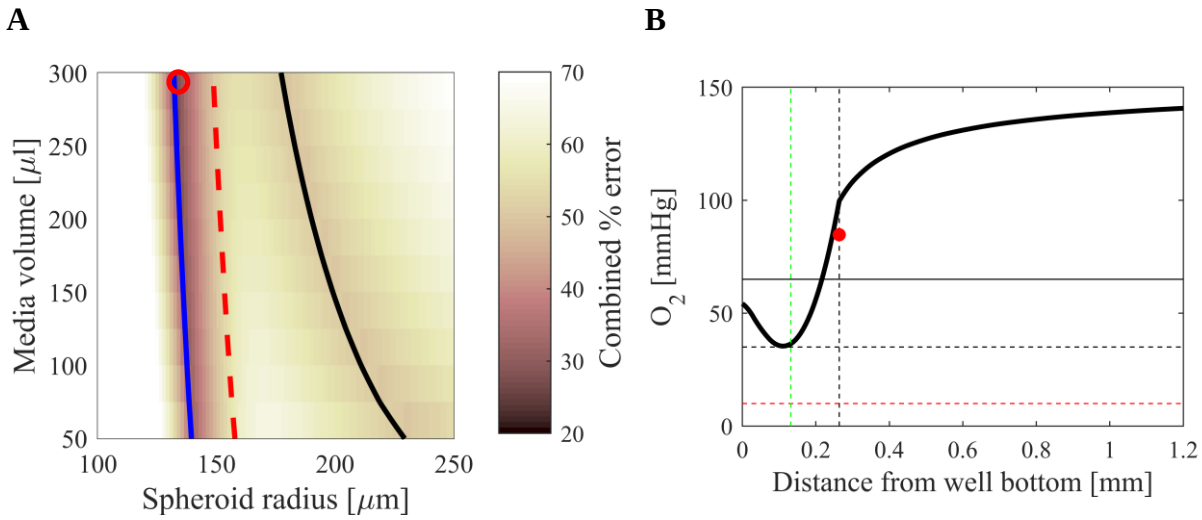

Figure 8: **Error calculation and minimisation in order to identify overall optimal *in vitro* culture conditions.** (A): Figure 7 contours for the optimal conditions that provide desired maximum spheroid oxygen concentration (solid, black), minimum spheroid oxygen concentration (solid, blue) and hypoxia (dashed, red) are collated onto a single plot. This plot shows the overall optimal operating conditions for the relevant ranges of spheroid radii and media volume through the calculation of a combined % error. The minimum error is indicated by a red circle. Note that in order to prevent hypoxia, the operating conditions should lie to the left of the hypoxic threshold. (B): The 1D oxygen profile corresponding to the minimum error parametrisation (red circle, (A)), is plotted with the same format and annotations as in Figure 6. The red dot indicates the average spheroid boundary concentration around the entire spheroid.

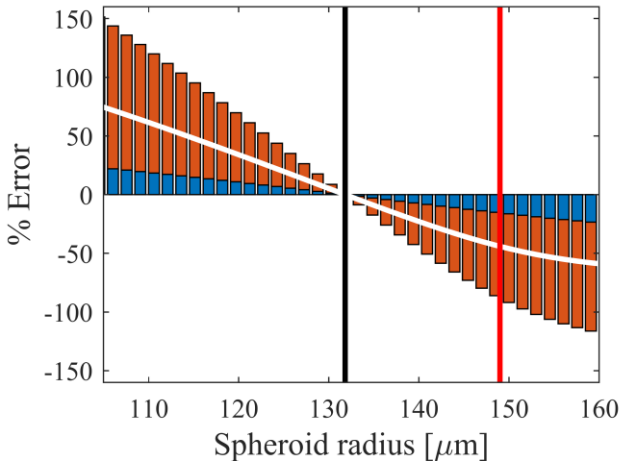

Figure 9: **Error sensitivity analysis of the optimal operating conditions proposed by Model II for HepG2 spheroids.** The percentage error for both the minimum oxygen concentration (red) and the maximum boundary concentration (blue) in the spheroid are plotted for variations in the optimal spheroid radius (131.82 μm) in 300 μl of media. An average error is also indicated (white line). The optimal spheroid radius to recapitulate the oxygen gradient (black line) and radius threshold for hypoxia (red line) are also shown.

4 Discussion

Optimisation of the *in vitro* hepatic spheroid system requires that culture conditions are calibrated such that physiologically relevant oxygen ranges are established. Mathematical models provide a means of testing the system in order to optimise physical system parameters in order to obtain desired system properties and consequently guide the process of 3D *in vitro* study design. Specifically, a model that is properly parameterised for intrinsic physiological processes (e.g. oxygen consumption rate, diffusion rate of oxygen) can be used to identify and optimise parameters such as media volume or spheroid radius that lead to the establishment of the *in vivo*-like hepatic sinusoid oxygen gradient. Consequently, such *in silico* models directly inform the design of experiments aiming to reproduce liver physiology *in vitro*.

Several insightful results regarding the optimal culture conditions have been acquired through the development and analysis of two mechanistic mathematical models, parameterised using experimental data. Provided one could ensure the fixed physiological oxygen concentration at

462 the spheroid boundary, Model I predicts that sinusoid gradients can be achieved for HepaRG
463 and HepG2 spheroids of radii 100 μm and 170 μm respectively (with the onset of hypoxia
464 occurring at 142 μm and 241 μm). HepG2 spheroids can afford to grow to a larger size without
465 experiencing hypoxia due to the reduced demand for oxygen (lower oxygen consumption rate,
466 V_{max}). This lower demand in oxygen may be due to the finding that in their unstressed state,
467 HepG2 cells produce cellular energy from both oxidative phosphorylation and anaerobic
468 glycolysis, due to the Warburg effect, and thus a reduced oxygen consumption rate is measured
469 due to the additional production of ATP via glycolysis (Kamalian et al., 2018). Conversely,
470 HepaRG cells only produce ATP via oxidative phosphorylation in the unstressed state and so
471 would need to consume more oxygen to produce the same amount of ATP. However, Model I
472 assumes the spheroid is cultured in a 3D radially symmetric environment whereas this
473 assumption is not valid in most experimental models. The extension of Model II to a more
474 realistic well geometry means that the precise end-points of the *in vivo* sinusoid gradient cannot
475 simultaneously be satisfied for any given combination of spheroid radius and media depth
476 combination. Therefore, culture conditions are identified by the model that minimise the
477 potential error of the end-points at the average spheroid boundary and minimum oxygen value
478 within the spheroid. This optimisation corresponds to a HepaRG spheroid radius of 132 μm
479 (with a revised hypoxic threshold of 149 μm) and 300 μl of media volume, which is in contrast
480 with more common instructions for culturing spheroids in 100 μl media (Korff, 2004, Charoen
481 et al., 2014, Morrison et al., 2016). However, the model oxygen gradient is more sensitive to
482 the spheroid radius parameter, and thus careful consideration should be given for spheroids that
483 change size over the defined culture period. In particular, sensitivity analysis reveals that small
484 perturbations in spheroid radius can lead to larger average errors in the gradient, relative to the
485 perturbation, and therefore precision is required to avoid the onset of hypoxia while preserving
486 central vein values. The application of both Models I and II suggest that there is a difference

in predicted optimal spheroid size when you take into account well geometry and oxygen diffusion through the media.

Another cell culture system currently used within the field comprises a multi-well plate with a gas-permeable bottom, covered with agarose to form U-shaped layer. This system is designed to improve the delivery of oxygen to multicellular spheroids and prevent necrosis in the centre of the spheroid. This feature, in combination with a U-shaped agarose layer, could alleviate the asymmetry of the oxygen profile in ULA plates. This alternative system was therefore implemented within our mathematical modelling framework by replicating the geometry for Model II with the further addition of 100 μl of agarose to form a U-shaped layer with a flat, gas-permeable bottom at the bottom of the well (for details of the investigation, see Supplementary Material). The results of this study (complementary to that of the ULA plate) showed that indeed, while symmetry was improved and larger non-hypoxic spheroids could be cultured, it was still not possible to achieve the desired *in vivo* gradient exactly. Model analysis identified a desired central oxygen concentration of 35 mmHg for an optimised 145.45 μm radius spheroid in 300 μl media. However, oxygen at the spheroid boundary, whilst relatively homogenous compared with the ULA plate system, remained too high for atmospheric external oxygen tensions.

The calibration and optimisation of intra-spheroidal oxygen profiles may also be improved via the controlled regulation of oxygen tensions within a cell culture incubator. The presented work has focused on the atmospheric oxygen levels commonly utilised within cell culture experiments. However, these non-physiological levels could result in hyperoxia if the media volume or spheroid size is insufficient (Gomes et al., 2016). Indeed, this issue can be seen for such scenarios as simulated by our model (e.g., Figure 7). Additionally, the use of further alternative cell culture formats may improve recapitulation of the *in vivo* sinusoid gradient in

hepatic spheroids. It is possible that the geometry of the hanging drop system would provide a more uniform, symmetric oxygen profile; however, this system uses a very small volume of liquid and so issues regarding waste products, medium changes and tight control of the oxygen environment must be considered. The culture of multiple small aggregates in a single well has also been shown to influence the oxygen distribution and lower steady state values and could therefore potentially be used as an optimisation tool (Lesher-Pérez et al., 2017).

Mathematical models comprise a useful tool for simulating physical problems, testing hypotheses *in silico*, and guiding subsequent experimental work. However, they are inherently simplified and abstract for tractability, and while driven by experimental data for calibration, it is also important to acquire feedback in the form of empirical data and continue model refinement. Thus, successful (i.e., useful) models (both mathematical and experimental) are the result of the iterative cycle between *in silico* and *in vitro* work. This model was implemented to thoroughly and efficiently analyse the physical and mechanistic conditions that influence spatial oxygen distribution in hepatic spheroids in view of commonly practised cell culture methodologies. The model simulates outputs that are inefficient and difficult to comprehensively obtain *in vitro*, but would now benefit from testing and verification experiments including local, real-time measurements of oxygen and evidence of hypoxic levels within the spheroid under specified scenarios.

Many previous *in silico* models have focused on oxygen kinetics in spheroids, highlighting the importance of properly characterising these mechanisms that describe the underlying biophysical processes. Most of these models rely on symmetrical properties or biochemical parameters derived from tumour spheroids. Such modelling work covers a range of applications that ultimately emphasise the need for optimisation of these *in vitro* systems, whether through the optimisation of spheroid morphology (Leung et al., 2015), defining optimal spheroid viability and functionality (Glicklis et al., 2004), or accounting for perfusion velocity and flow

within microbioreactors (Allen & Bhatia, 2003, Hu & Li, 2007, Barisam et al., 2018). Some key novelties arising from our multidisciplinary modelling work include the measurement of oxygen uptake parameters that are integrated into mathematical models to generate bespoke dynamics for both HepG2 and HepaRG cell lines; the development and parameterisation of a model that takes into account a realistic ULA geometry with, most importantly, asymmetry; and an improved guide for media volume conditions in these environments relevant to hepatic spheroid culture. The utility of this spheroid mathematical modelling framework can be further extended to incorporate drug transport and metabolism components in a similar approach, ultimately providing a more realistic description of the environment and culturing conditions used *in vitro* for improved medical applications.

Acknowledgements

The work was supported by the National Centre for the Replacement, Refinement and Reduction of Animals in Research (NC3Rs) CRACK-IT fund, Challenge 5: IVIVE. JL, RNB and SDW acknowledge funding support from the Liverpool Centre for Mathematics in Healthcare (EPSRC grant: EP/N014499/1). JL is supported by an MRC Skills Development Fellowship (MR/S019332/1).

Author contributions

JL wrote the manuscript; JL, RNB & SDW contributed to the mathematical modelling; AEC, HEC & CM contributed to the experimental inputs; HG, DPW & SDW designed the research. SDW directed the research. All authors read and approved the final manuscript.

Declaration of interests

The authors declare that they have no competing interests.

References

Allen J W and Bhatia S N (2003) Formation of steady-state oxygen gradients in vitro: Application to liver zonation. *Biotechnology and bioengineering* 82: 253-262.

Anada T, Fukuda J, Sai Y and Suzuki O (2012) An oxygen-permeable spheroid culture system for the prevention of central hypoxia and necrosis of spheroids. *Biomaterials* 33: 8430-8441.

Barisam M, Saidi M S, Kashaninejad N and Nguyen N-T (2018) Prediction of Necrotic Core and Hypoxic Zone of Multicellular Spheroids in a Microbioreactor with a U-Shaped Barrier. *Micromachines* 9: 94.

Brown J M and Giaccia A J (1998) The unique physiology of solid tumors: opportunities (and problems) for cancer therapy. *Cancer research* 58: 1408-1416.

Buerk D G and Saidel G M (1978) Local kinetics of oxygen metabolism in brain and liver tissues. *Microvascular research* 16: 391-405.

Carmeliet P and Jain R K (2000) Angiogenesis in cancer and other diseases. *nature* 407: 249.

Carreau A, Hafny-Rahbi B E, Matejuk A, Grillon C and Kieda C (2011) Why is the partial oxygen pressure of human tissues a crucial parameter? Small molecules and hypoxia. *Journal of cellular and molecular medicine* 15: 1239-1253.

Chaplain M (1996) Avascular growth, angiogenesis and vascular growth in solid tumours: The mathematical modelling of the stages of tumour development. *Mathematical and computer modelling* 23: 47-87.

Charoen K M, Fallica B, Colson Y L, Zaman M H and Grinstaff M W (2014) Embedded multicellular spheroids as a biomimetic 3D cancer model for evaluating drug and drug-device combinations. *Biomaterials* 35: 2264-2271.

Colley H E, Hearnden V, Avila-Olias M, Cecchin D, Canton I, Madsen J, MacNeil S, Warren N, Hu K and McKeating J A (2014) Polymersome-mediated delivery of combination anticancer therapy to head and neck cancer cells: 2D and 3D in vitro evaluation. *Molecular pharmaceutics* 11: 1176-1188.

Colton C K (1995) Implantable biohybrid artificial organs. *Cell transplantation* 4: 415-436.

Corning Life Sciences. (2018). "Life Sciences Products and Equipment." Retrieved 8 Oct, 2018, from http://www.corning.com/lifesciences/.

598
599 Curcio E, Salerno S, Barbieri G, De Bartolo L, Drioli E and Bader A (2007) Mass transfer and
600 metabolic reactions in hepatocyte spheroids cultured in rotating wall gas-permeable membrane
601 system. *Biomaterials* 28: 5487-5497.

602
603 Foy B D, Rotem A, Toner M, Tompkins R G and Yarmush M L (1994) A device to measure
604 the oxygen uptake rate of attached cells: importance in bioartificial organ design. *Cell*
605 *Transplantation* 3: 515-527.

606
607 Freyer J P (1988) Role of necrosis in regulating the growth saturation of multicellular
608 spheroids. *Cancer research* 48: 2432-2439.

609
610 Glicklis R, Merchuk J C and Cohen S (2004) Modeling mass transfer in hepatocyte spheroids
611 via cell viability, spheroid size, and hepatocellular functions. *Biotechnology and*
612 *bioengineering* 86: 672-680.

613
614 Gomes A, Guillaume L, Grimes D R, Fehrenbach J, Lobjois V and Ducommun B (2016)
615 Oxygen partial pressure is a rate-limiting parameter for cell proliferation in 3d spheroids grown
616 in physioxic culture condition. *PloS one* 11: e0161239.

617
618 Grimes D R, Kelly C, Bloch K and Partridge M (2014a) A method for estimating the oxygen
619 consumption rate in multicellular tumour spheroids. *J R Soc Interface* 11: 20131124.

620
621 Grimes D R, Fletcher A G and Partridge M (2014b) Oxygen consumption dynamics in steady-
622 state tumour models. *Royal Society Open Science* 1: 140080.

623
624 Grimes D R, Kannan P, McIntyre A, Kavanagh A, Siddiky A, Wigfield S, Harris A and
625 Partridge M (2016) The role of oxygen in avascular tumor growth. *PloS one* 11: e0153692.

626
627 Gunness P, Mueller D, Shevchenko V, Heinzle E, Ingelman-Sundberg M and Noor F (2013)
628 3D organotypic cultures of human HepaRG cells: a tool for in vitro toxicity studies.
629 *Toxicological sciences* 133: 67-78.

630
631 Hu G and Li D (2007) Three-dimensional modeling of transport of nutrients for multicellular
632 tumor spheroid culture in a microchannel. *Biomedical microdevices* 9: 315-323.

633
634 Jungermann K and Keitzmann T (1996) Zonation of parenchymal and nonparenchymal
635 metabolism in liver. *Annual review of nutrition* 16: 179-203.

636
637 Jungermann K and Kietzmann T (2000) Oxygen: modulator of metabolic zonation and disease
638 of the liver. *Hepatology* 31: 255-260.

Kamalian L, Douglas O, Jolly C E, Snoeys J, Simic D, Monshouwer M, Williams D P, Park B K and Chadwick A E (2018) The utility of HepaRG cells for bioenergetic investigation and detection of drug-induced mitochondrial toxicity. *Toxicology in Vitro* 53: 136-147.

Kietzmann T (2017) Metabolic zonation of the liver: The oxygen gradient revisited. *Redox biology* 11: 622-630.

Korff T (2004). Three-dimensional in vitro angiogenesis assays. Methods in Endothelial Cell Biology, Springer**:** 115-123.

Kyffin J A, Sharma P, Leedale J, Colley H E, Murdoch C, Mistry P and Webb S D (2018) Impact of cell types and culture methods on the functionality of in vitro liver systems-A review of cell systems for hepatotoxicity assessment. *Toxicology In Vitro* 48: 262-275.

Lee-Montiel F T, George S M, Gough A H, Sharma A D, Wu J, DeBiasio R, Vernetti L A and Taylor D L (2017) Control of oxygen tension recapitulates zone-specific functions in human liver microphysiology systems. *Experimental Biology and Medicine* 242: 1617-1632.

Lee S H, Do S-I and Kim H-S (2014) Hyperoxia accelerates progression of hepatic fibrosis by up-regulation of transforming growth factor-β expression. *World Journal of Gastroenterology: WJG* 20: 3011.

Leedale J, Herrmann A, Bagnall J, Fercher A, Papkovsky D, Sée V and Bearon R N (2014) Modeling the dynamics of hypoxia inducible factor-1α (HIF-1α) within single cells and 3D cell culture systems. *Mathematical biosciences* 258: 33-43.

Lesher-Pérez S C, Kim G-A, Kuo C-h, Leung B M, Mong S, Kojima T, Moraes C, Thouless M, Luker G D and Takayama S (2017) Dispersible oxygen microsensors map oxygen gradients in three-dimensional cell cultures. *Biomaterials science* 5: 2106-2113.

Leung B M, Lesher-Perez S C, Matsuoka T, Moraes C and Takayama S (2015) Media additives to promote spheroid circularity and compactness in hanging drop platform. *Biomaterials science* 3: 336-344.

Lodish H, Berk A, Zipursky S L, Matsudaira P, Baltimore D and Darnell J (2000). Molecular cell biology, WH Freeman New York.

Martinez I, Nedredal G I, Øie C I, Warren A, Johansen O, Le Couteur D G and Smedsrød B (2008) The influence of oxygen tension on the structure and function of isolated liver sinusoidal endothelial cells. *Comparative hepatology* 7: 4.

Mattei G, Magliaro C, Giusti S, Ramachandran S D, Heinz S, Braspenning J and Ahluwalia A (2017) On the adhesion-cohesion balance and oxygen consumption characteristics of liver organoids. *PloS one* 12: e0173206.

Mehta G, Hsiao A Y, Ingram M, Luker G D and Takayama S (2012) Opportunities and challenges for use of tumor spheroids as models to test drug delivery and efficacy. *Journal of Controlled Release* 164: 192-204.

Morrison E, Wai P, Leonidou A, Bland P, Khalique S, Farnie G, Daley F, Peck B and Natrajan R (2016) Utilizing functional genomics screening to identify potentially novel drug targets in cancer cell spheroid cultures. *Journal of visualized experiments: JoVE*.

Muz B, de la Puente P, Azab F and Azab A K (2015) The role of hypoxia in cancer progression, angiogenesis, metastasis, and resistance to therapy. *Hypoxia* 3: 83.

Nyberg S L, Remmel R P, Mann H J, Peshwa M V, Hu W-S and Cerra F B (1994) Primary hepatocytes outperform Hep G2 cells as the source of biotransformation functions in a bioartificial liver. *Annals of surgery* 220: 59.

Olive P L, Vikse C and Trotter M J (1992) Measurement of oxygen diffusion distance in tumor cubes using a fluorescent hypoxia probe. *International Journal of Radiation Oncology* Biology* Physics* 22: 397-402.

Rangan S (1972) A new human cell line (FaDu) from a hypopharyngeal carcinoma. *Cancer* 29: 117-121.

Riffle S and Hegde R S (2017) Modeling tumor cell adaptations to hypoxia in multicellular tumor spheroids. *Journal of Experimental & Clinical Cancer Research* 36: 102.

Shipley R, Davidson A J, Chan K, Chaudhuri J B, Waters S and Ellis M J (2011) A strategy to determine operating parameters in tissue engineering hollow fiber bioreactors. *Biotechnology and bioengineering* 108: 1450-1461.

Vaupel P, Kallinowski F and Okunieff P (1989) Blood flow, oxygen and nutrient supply, and metabolic microenvironment of human tumors: a review. *Cancer research* 49: 6449-6465.

Ward J P and King J R (2003) Mathematical modelling of drug transport in tumour multicell spheroids and monolayer cultures. *Mathematical biosciences* 181: 177-207.

Williams D P, Shipley R, Ellis M J, Webb S, Ward J, Gardner I and Creton S (2013) Novel in vitro and mathematical models for the prediction of chemical toxicity. *Toxicology research* 2: 40-59.

Yamada K M and Cukierman E (2007) Modeling tissue morphogenesis and cancer in 3D. *Cell* 130: 601-610.

Yarmush M, Toner M, Dunn J, Rotem A, Hubel A and Tompkins R (1992) Hepatic tissue engineering: Development of critical technologies. *Annals of the New York Academy of Sciences* 665: 238-252.